Development and Characterization of a 96-Well Exposure System for Safety Assessment of Nanomaterials

Yvonne Kohl,* Michelle Müller, Marielle Fink, Marc Mamier, Siegfried Fürtauer, Roland Drexel, Christine Herrmann, Stephan Dähnhardt-Pfeiffer, Ramona Hornberger, Marius I. Arz, Christoph Metzger, Sylvia Wagner, Sven Sängerlaub, Heiko Briesen, Florian Meier, and Tobias Krebs

In this study, a 96-well exposure system for safety assessment of nanomaterials is developed and characterized using an air–liquid interface lung epithelial model. This system is designed for sequential nebulization. Distribution studies verify the reproducible distribution over all 96 wells, with lower insert-to-insert variability compared to non-sequential application. With a first set of chemicals (TritonX), drugs (Bortezomib), and nanomaterials (silver nanoparticles and (non-)fluorescent crystalline nanocellulose), sequential exposure studies are performed with human lung epithelial cells followed by quantification of the deposited mass and of cell viability. The developed exposure system offers for the first time the possibility of exposing an air–liquid interface model in a 96-well format, resulting in high-throughput rates, combined with the feature for sequential dosing. This exposure system allows the possibility of creating dose-response curves resulting in the generation of more reliable cell-based assay data for many types of applications, such as safety analysis. In addition to chemicals and drugs, nanomaterials with spherical shapes, but also morphologically more complex nanostructures can be exposed sequentially with high efficiency. This allows new perspectives on in vivo-like and animal-free approaches for chemical and pharmaceutical safety assessment, in line with the 3R principle of replacing and reducing animal experiments.

1. Introduction

Due to the coronavirus disease 2019 pandemic, research on lung diseases and the development of sophisticated lung models have become even more important. The need for models and new techniques for the development of new drugs, especially inhalable drugs, is growing steadily.[1] It is apparent, not only in the field of therapy development, but also in the field of risk assessment of air pollutants – such as particulate matter, dusts, nanoparticles, and chemicals—that there is a great need for test systems that reflect the "real" situation of pollutant exposure or inhalation, both from the biological and the technical application side.[2]

In addition, due to ethical aspects and political demands, animal models in pharmaceutical and toxicological testing are being increasingly replaced by animal-free methods, such as advanced in vitro models. Within the scope of the 3R principle of Russell and Burch (replace, reduce, refine),[3] compliance is becoming mandatory in

Y. Kohl, M. Müller, S. Wagner
Bioprocessing & Bioanalytics
Fraunhofer Institute for Biomedical Engineering IBMT
Joseph-von-Fraunhofer-Weg 1, 66280 Sulzbach, Germany
E-mail: yvonne.kohl@ibmt.fraunhofer.de

M. Fink, M. Mamier, T. Krebs
VITROCELL Systems GmbH
Fabrik Sonntag 3, 79183 Waldkirch, Germany

ⓘ The ORCID identification number(s) for the author(s) of this article can be found under https://doi.org/10.1002/smll.202207207.

S. Fürtauer, R. Hornberger, M. I. Arz,[+] S. Sängerlaub
Materials Development
Fraunhofer Institute for Process Engineering & Packaging IVV
Giggenhauser Str. 35, 85354 Freising, Germany

R. Drexel, F. Meier
Postnova Analytics GmbH
86899 Landsberg am Lech, Germany

C. Herrmann, C. Metzger, H. Briesen
Process Systems Engineering
School of Life Sciences
Technical University Munich
Gregor-Mendel-Str. 4, 85354 Freising, Germany

S. Dähnhardt-Pfeiffer
Microscopy Services Dähnhardt GmbH
Plambeckskamp 2, 24220 Flintbek, Germany

ADVANCED
SCIENCE NEWS
www.advancedsciencenews.com

NANO · MICRO
small
www.small-journal.com

Europe and worldwide in the execution of pharmaceutical and toxicological studies.[4–6]

In order to meet this challenge, not only in vitro models, but also technical application systems combined with the in vitro models must be developed further.

During the last several years, a significant number of advanced in vitro lung models (co-cultures, multi cultures, primary cultures, 3D cultures, organoids, or models based on induced pluripotent stem cells)[1,7–17] have been developed; as they bring distinct advantages such as relevance to human physiology, cost effectiveness, and handling. Nevertheless, many in vitro test methods are not yet complex enough to replace the process of "inhalation" as a whole.[7,18] Due to its complexity, mechanical devices have been combined with biological models, thereby enabling the exposure of gas or aerosols to cells cultured at an air-liquid–interface (ALI).[2] Until today, most devices that allow "physiological" aerosol exposure of cells have been based on the sedimentation principle, which facilitates cell exposure with the test substance only as non-sequential aerosol exposure and only for up to 48 positions at the same time.[2,19–25] When using the flow principle, the maximum number of positions exposed in parallel is limited to 48 samples.[21,26] To date, no exposure system has been developed to enable a sequential exposure of ALI models in a high-throughput format, such as a 96-well plate.

To simulate the inhalation process in vitro nebulizers are used for aerosolization of liquid drugs, as they provide a moderate, continuous flow rate and a constant aerosol size distribution in the optimal range for pulmonary or nasal delivery.[27] Choosing a nebulizer exerting low shear forces during aerosol generation can reduce aggregation and loss of bioactivity.[28–30]

This is also of special relevance in the field of nanosafety assessment of inhalable dusts and nanomaterials.[21,31] Lung diseases, such as pneumoconiosis or allergic alveolitis, are caused by the inhalation of dusts with subsequent deposition in the lungs as well as tissue reaction.[32,33] In addition to dusts, which are solid microparticles, numerous nanomaterials, and particulate matter also trigger inflammation and other diseases in the lungs.[34] These findings are largely based on in vivo studies.[35,36]

At present, there are no validated systems for aerosol application of drugs or nanomaterials in a high-throughput format and for the rapid determination of effect thresholds. Such systems would be of great help in the field of occupational hazard potential analysis and in the risk assessment of new materials in the micro- and nanoscale regime, such as cellulose nanocrystals (CNC) for example.[37–42] Although CNC are already used on a commercial scale, little is known so far about their potential biological effects after inhalation. This particle type can act as a good example for several new materials with complex morphology, whose effects on inhalation need to be studied. Due to the lack of validated in vitro methods and application technologies in a high-throughput format, such studies are currently performed only in vivo.[36,43–45] Against this background there is a great need for advanced technologies for assessing a dose-response relationship of new inhalable materials in a fast and reproducible manner.

Cloud technology represents a promising approach for sequential ALI exposure with aerosols in a 96-well format.

The first prototype of cloud technology was introduced in 2009 by Lenz et al.,[46] followed by a detailed characterization of a refined, commercially available system, Cloud 6, which was subsequently extended by versions with 12 and 24 inserts.[46,47] The application of this cloud system for in vitro aerosol exposure studies of chemicals,[48–50] dust, and gas[49,51–54] as well as nanoparticles[55–62] has already been successfully demonstrated. While the cloud system SEQ 24 has been characterized for application in cell experiments,[19,63] the effect of the miniaturization of the format (24-well to 96-well) on the distribution of the nebulized substances, the cultivation of the cells, as well as the effect efficiency of the test substance, is unclear. In this study, an aerosol exposure system for dose-response studies of drugs and nanoparticles on an ALI lung epithelial model, in a 96-well format, was fabricated and characterized using reference drugs and nanomaterials.

2. Results and Discussion

2.1. Setup of the Sequential 96-Well Exposure System

A 96-well exposure system for nebulization of substances was manufactured. The developed system provides aerosol exposure for ALI cell models to chemicals, drugs, and nanomaterials or other active substances, in aerosolized form, under controlled and reproducible conditions. It features ease of operation and reliable exposure. Compared to the 6-, 12- and 24-well format, the 96-well design allows testing at high-throughput rates, combined with the feature of sequential dosing on each of the 12 rows of well, offering the possibility of creating dose-response curves. This exposure system consists of nine different components (**Figure 1**). The nebulizer and the mounting of the nebulizer with the vacuum outlet are placed on the aerosol chamber. The sliding panel can be moved manually across the base module. The base module consists of a flat,
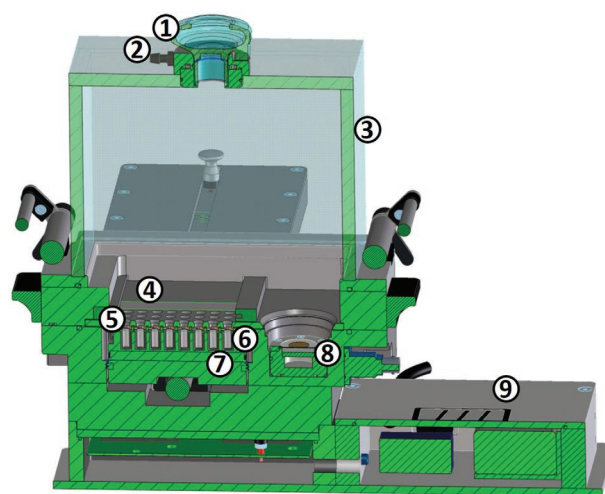

Figure 1. Schematic set-up of the 96-well exposure system. 1) nebulizer, 2) mounting of the nebulizer with vacuum outlet, 3) aerosol chamber, 4) sliding panel, 5) flat 96-well stainless steel plate, 6) 96-well insert plate, 7) 96-well stainless steel plate, 8) quartz crystal microbalance, 9) temperature control unit.
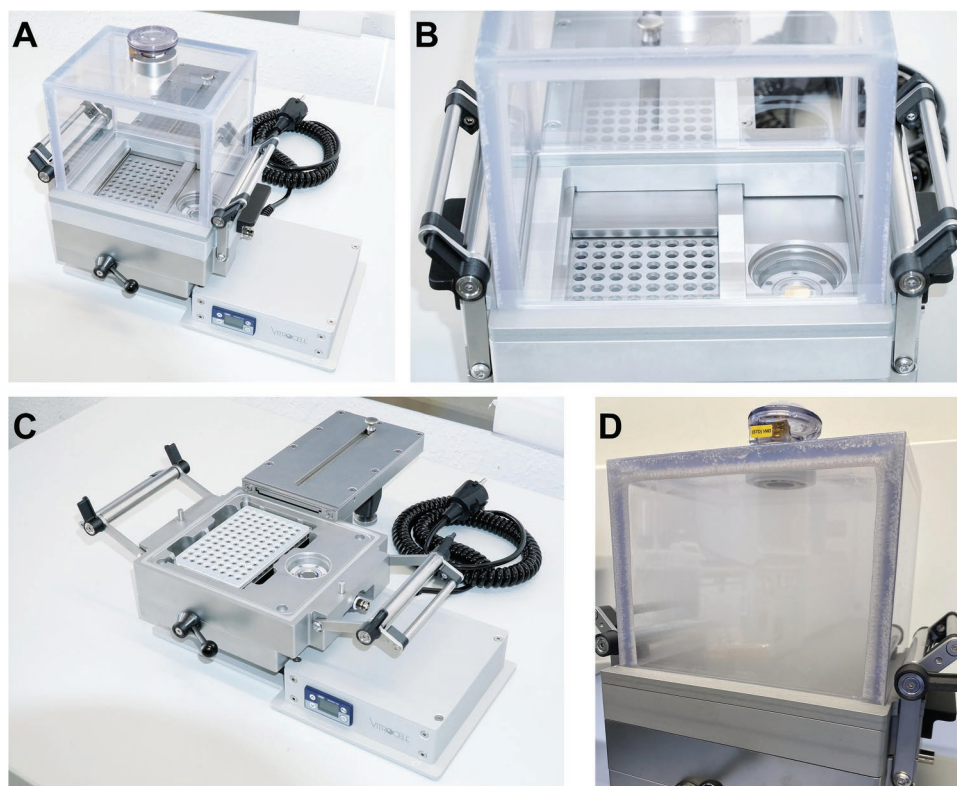
Figure 2. 96-well exposure system. A) completely assembled system, B) 96-well stainless steel plate with sliding panel and quartz crystal microbalance, C) complete system without aerosol chamber, D) formed mist in the aerosol chamber.

96-well stainless steel plate that covers the 96-well insert plate. This is then placed onto a second, 96-well stainless steel plate that contains the basal cell culture medium. The base module holds another insert for the 6-well quartz crystal microbalance (QCM) and can be used to heat the cells up to physiological temperatures, with a temperature control unit (Figure 1 and **Figure 2**).

The basic principle of the cloud system has been previously described in detail.[47] In brief, cells are grown on cell culture inserts, which are placed at the bottom of the exposure chamber. A solution of the test substance is placed on the vibrating mesh nebulizer located on the top of the chamber. The test liquid passes the vibrating mesh nebulizer resulting in the formation of a dense cloud of droplets. Subsequent sedimentation results in uniform aerosol deposition onto the cells, which are located in inserts at the bottom of the exposure chamber. A QCM in the base module facilitates accurate dosimetry measurement of the deposited mass onto the cells.[47,64]

The developed exposure system allows exposure to aerosols using a 96-well format for the first time, resulting in high-throughput rates. This is combined with the feature for sequential dosing of each of the 12 rows of well, which offers the possibility of creating dose-response curves with an aerosol exposure system. The characterization of drug and nanoparticle distribution as well as in vitro studies on dose response in a 96-well format has not yet been reported. This application has previously been reported using a 12-well exposure system.[65] For the characterization of the 96-well exposure system, a stepwise approach was taken, using chemicals and nanomaterials in each case. In the first step, distribution studies were performed with fluorescein sodium and fluorescence-labeled crystalline nanocellulose (CNC). In the second step, ALI models were sequentially exposed to chemicals or nanomaterials, followed by later determination of cell viability.

2.2. Nanoparticles for System Characterization

In addition to known reference chemicals and pharmaceuticals, nanoparticles with a spherical shape as well as nanoparticles with a complex morphological structure were used to characterize the 96-well exposure system. As an example of the latter, CNC was synthesized and labeled with a fluorescent dye. The characteristics of the labeled and unlabeled CNC are described in detail in the supplementary material. In brief, CNC was extracted from hardwood pulp by sulfuric acid hydrolysis and fluorescently labeled with AlexaFluor (AF) 488 (CNC-AF488) by treating the CNC with 3-aminopropyltriethoxysilane (APTES) and AF 488 NHS ester. For physicochemical characterization, ζ-potential, mean hydrodynamic diameter (using batch DLS), and gyration radius (using asymmetrical-flow field-flow fractionation coupled with multi angle light scattering (AF4-MALS)) were determined (**Table 1**, Tables S1,S2 and Figure S1, Supporting Information). Successful conjugation of AF488 was demonstrated by FTIR spectroscopy (Figure S2 and Table S3, Supporting Information).

Table 1. Physico-chemical characteristics of CNC and CNC-AF488 in the stock solution.

Nanoparticle	Size [nm]/DLS	Size [nm]/AF4-MALS	ζ-potential [mV]	PDI
CNC	140.0 ± 1.0	136.0 ± 0.2	-39.0 ± 1.0	0.402 ± 0.009
CNC-AF488	151.0 ± 1.5	196.6 ± 8.9	-3.9 ± 0.5	0.240 ± 0.008

Further evidence of the particle characteristics of the CNC was provided by transmission electron microscopic (TEM) analysis. CNC and CNC-AF488 show characteristic fiber-like structures, which are distinguishable from each other, showing no agglomeration. No differences in morphology or size ratio and distribution are evident between un-nebulized CNC and un-nebulized CNC-AF488. These findings are consistent with those described by Campora et al.[66] Also, no differences between nebulized and un-nebulized CNC are detectable either by coupling the fluorescence dye or by the process of nebulization (**Figure 3**). After threefold nebulization, larger clusters are visible, but particle shape and size correspond to un-nebulized material. Even after threefold nebulization, CNC and CNC-AF488 still correspond to the shape and size of the un-nebulized material (Figure 3).

2.3. Aerosol Distribution in the 96-Well Exposure System

2.3.1. Cell-Free Characterization with Fluorescein Sodium

For characterization and evaluation of the system, cell-free experiments with aerosolized fluorescein sodium solution

as a chemical/drug proxy were conducted. The system was tested in both, non-sequential mode (exposing all 96 positions once) and sequential mode (exposing single rows of well up to 12 times, resulting in 12 different dose levels). Spectrometric quantitative analysis of the deposited fluorescein sodium was performed. The QCM was not used in this experiment. For the non-sequential mode, the mean deposited mass of fluorescein sodium is 0.047 ± 0.007 µg cm^{-2} after a single exposure with 500 µL fluorescein sodium (30 µg mL^{-1}). For the sequential mode, the deposited mass ranges from 0.033 ± 0.002 µg cm^{-2} after one exposure with 500 µL fluorescein sodium (15 µg mL^{-1}) to 0.382 ± 0.015 µg cm^{-2} after 12 exposures. For 12 exposures in sequential mode a total volume of 6 mL fluorescein sodium (15 µg mL^{-1}) was used. Besides a significantly higher deposition efficiency (**Figure 4**A) the insert-to-insert variability is also significantly lower in the sequential mode (Figure 4B). In the case of the sequential mode, a uniform increase in the dose levels for each additional exposition could be detected (Figure 4C). These results verify that the sequential dosing feature is functional. As Steiner et al. previously showed for a cloud system SEQ 24, it is crucial for sequential operation to clean the chamber between the exposures to avoid contamination
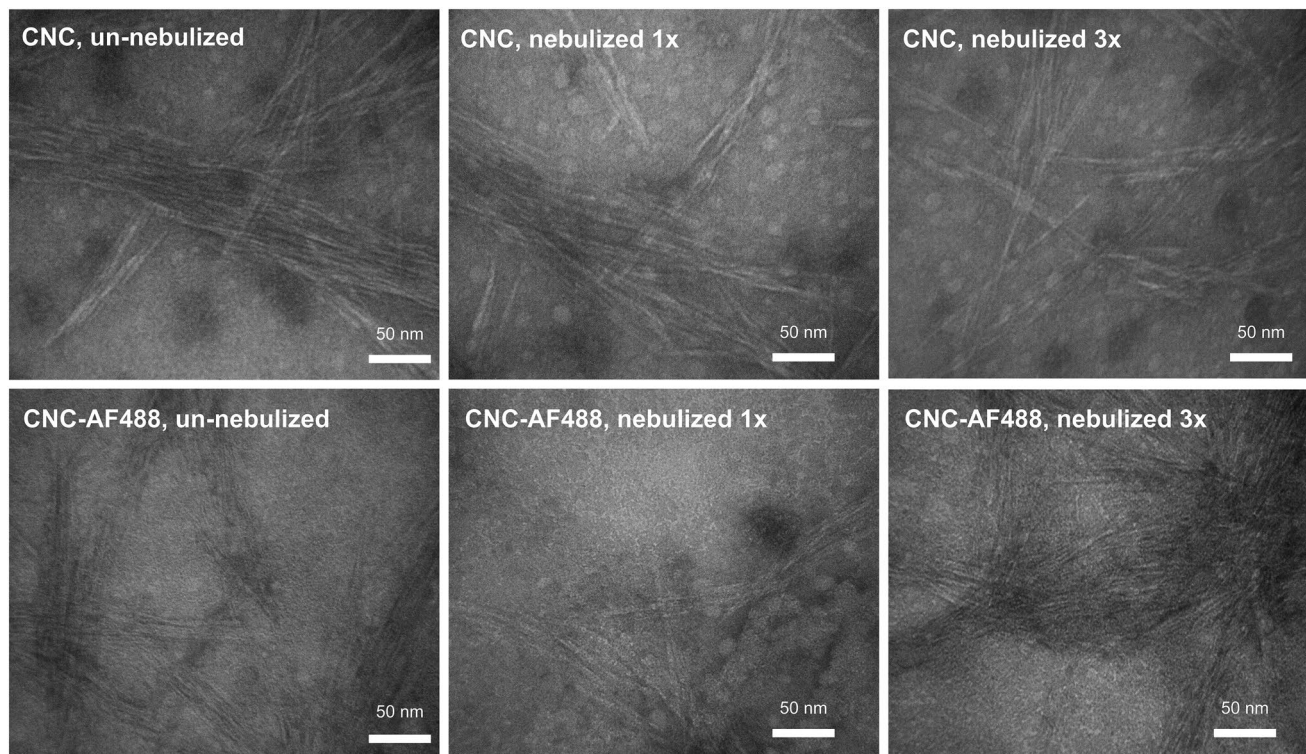

Figure 3. TEM images of CNC and CNC-AF488 un-nebulized and after nebulization. CNC and CNC-AF488 were analyzed before nebulization, after single, and after three times nebulization. Scale bar 50 nm.
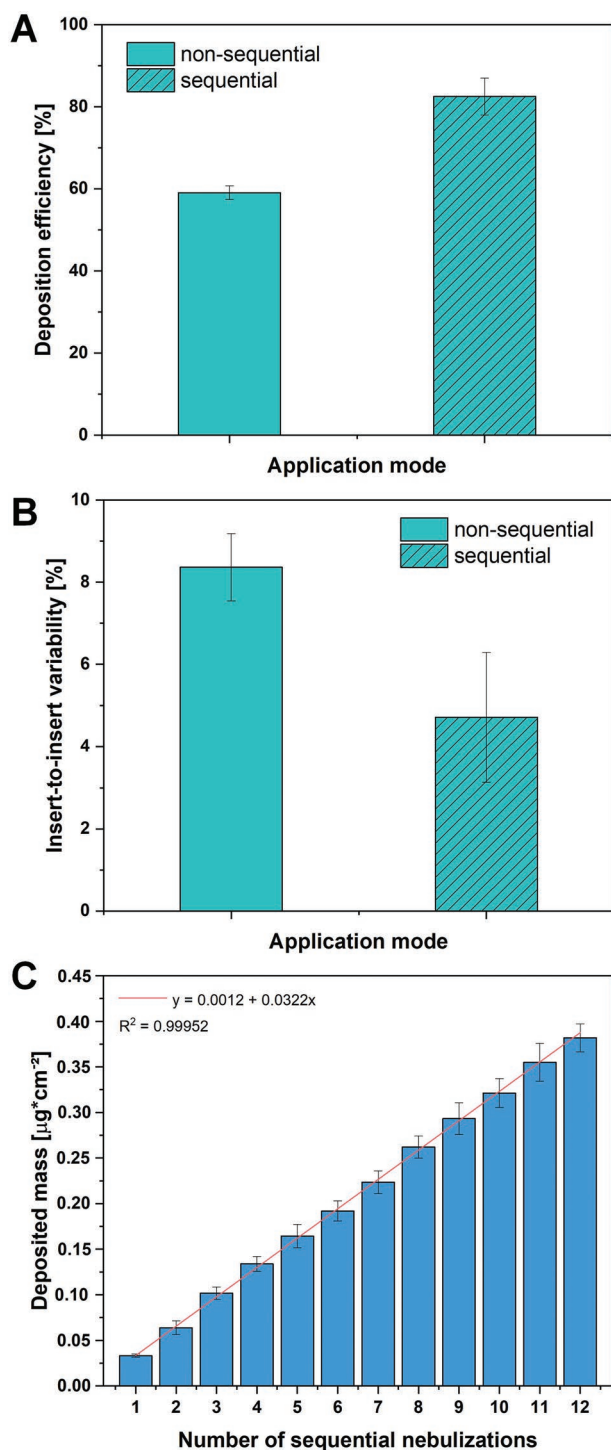
Figure 4. Delivery characteristics of the 96-well exposure system in cell-free experiments using a fluorescein sodium solution as a proxy drug. A) Deposition efficiency of non-sequential and sequential modes. Deposition efficiency of the non-sequential mode, meaning one exposure over all 96 positions, was lower compared to sequential mode. B) Insert-to-insert-variability of sequential and non-sequential modes. These values demonstrate highly uniform distribution of the aerosol between the inserts. C) Mean deposited mass of fluorescein sodium for 12 dose levels ($n = 3$). The uniform increase between the levels shows the functionality of the dosing feature for up to 12 doses.

due to electrical charge deposited on the chamber walls.[63] Data from the 96-well exposure system proves that applying a slight vacuum after each exposure is an alternative, faster and easier-to-handle method to remove residual aerosol between the exposures. The sedimentation time is driven by the two settling mechanisms which are cloud settling and single droplet sedimentation. As the particles are incorporated into the droplets the recommended settling time mainly depends on the droplet size. This is defined by the pore size of the mesh of the nebulizer. Based on theoretical cloud settling, that is, particle settling speed[46] and experimental QCM data,[64] a settling time of 5 min is conservatively recommended for the Cloud system. Thus, it can be assumed that >95% of the final deposited drug dose is delivered during the chosen settling time of 7 min for cell-free and 5 min for biological experiments before evacuation. From the deposited fluorescein dose the deposition efficiency of the cloud system was determined, indicating the percentage of the total nebulized fluorescein mass reaching the bottom of the exposure chamber after settling time, implicitly assuming spatially uniform aerosol deposition. Another important characteristic of the cloud systems is the insert-to-insert variability, representing the uniformity of the aerosol distribution in the inserts (Figure S5, Supporting Information).

Deposition efficiency and insert-to-insert variability for non-sequential and sequential modes of the 96-well exposure system are depicted in Figure 4A,B. Mean deposition efficiency for the non-sequential mode is 59.2 ± 1.7%. For the sequential mode, the average deposition efficiency of all 12 doses is 82.5 ± 4.5%. Mean insert-to-insert-variability for non-sequential mode and thus over 96 inserts is 8.4 ± 0.8% and 4.7 ± 1.6% for non-sequential mode over 8 inserts in one row. Comparing these values to previously reported data using fluorescein sodium to characterize the cloud exposure systems, deposition efficiency of the sequential mode of 82.5% is in the range of the values of 83.6% and 79.0% for the Cloud 6.[47,64] The slightly lower reported values of 68.0% for the Cloud 12 and 69.0% for Cloud 24 SEQ (non-sequential mode) may indicate, that higher losses might correlate with a decreased insert size, for example, due to higher losses at the insert-walls.[63,64] This could explain the comparable lower deposition efficiency of the non-sequential mode of 59.2%. The difference in the deposition efficiency of the non-sequential and the sequential mode might be explained by the two-fold higher concentrations of fluorescein sodium nebulized at once in the non-sequential mode. The higher concentration of nebulized fluorescein sodium might lead to proportionally higher losses, resulting in a lower deposition efficiency. However, insert-to-insert variability for non-sequential mode and sequential mode was lower than 10%, implying high uniformity and is in the range of 8.6% reported by Lenz et al. in 2014 for Cloud 6.[47] In conclusion, the cell-free experiments with fluorescein sodium demonstrate that the 96-well exposure system can be operated in non-sequential and sequential modes in a dose-controlled, highly reproducible manner with spatially uniform deposition (Figure S5, Supporting Information). The sequential dosing feature is functional for up to 12 doses (Table S4, Supporting Information).
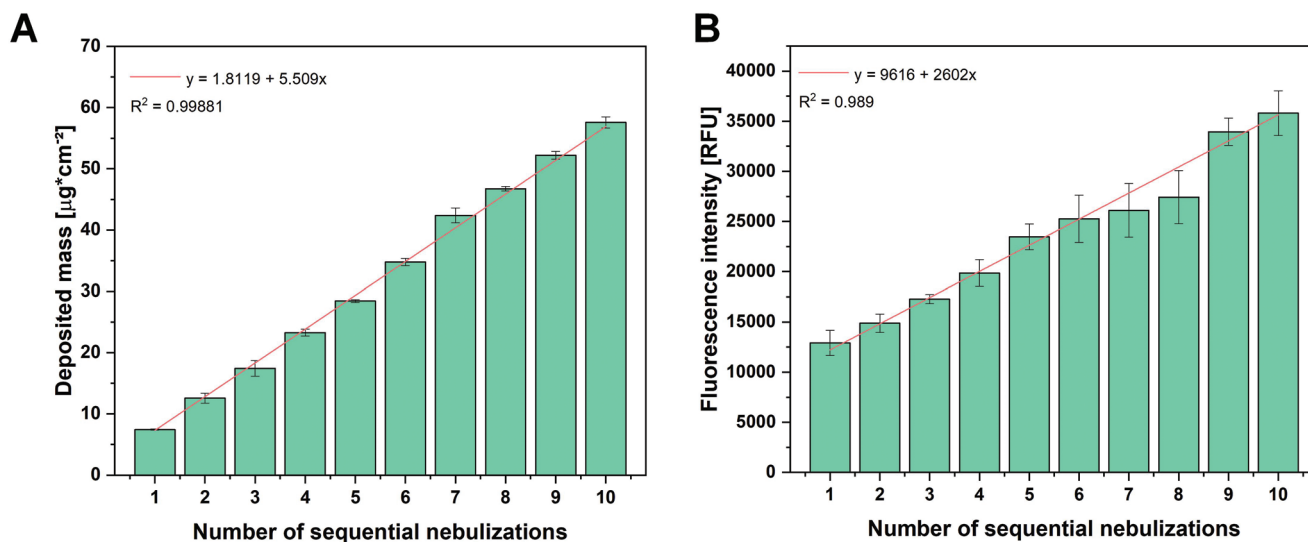
Figure 5. Nanomaterial delivery characteristics of the 96-well exposure system in cell-free experiments using fluorescent crystalline nanocellulose (CNC-AF488). A) Deposited mass of CNC-AF488 for 10 dose levels measured by QCM. The uniform increase between the levels also shows the functionality of the dosing feature for nanomaterials. B) Relative fluorescence intensity of CNC-AF488 for 10 dose levels. Mean values of three independent experiments ± standard deviation.

2.3.2. Cell-Free Characterization with Fluorescent CNC

Fluorescent CNC (CNC-AF488) was used for cell-free experiments in sequential mode (exposing single rows up to ten times, resulting in 10 dose levels). Mean deposited mass of CNC-AF488 for 10 dose levels was measured by QCM. The values range from 7.42 ± 0.09 µg cm^{-2} after one exposure to 61.68 ± 0.52 µg cm^{-2} after 10 exposures (**Figure 5**A). In parallel, the CNC-AF488 deposition efficiency was determined by measuring the fluorescence intensity in each well. The values range from $12\,910 \pm 1249$ relative fluorescent units (RFU) after one exposure to $35\,804 \pm 2221$ RFU after 10 exposures (Figure 5B).

As shown previously for chemicals, in a 24-well format,[63] the homogeneous distribution and sequential aerosol application of nanostructures could be clearly verified in the 96-well exposure system. In conclusion, the cell-free experiments with CNC-AF488 demonstrated the suitability of the 96-well exposure system for sequential mode in a dose-controlled, highly reproducible manner, with spatially uniform deposition.

2.4. In Vitro Studies after Exposure in the 96-Well Exposure System

After a very homogeneous distribution of the nebulized test materials in the individual wells could be verified, the in vitro application of the exposure system was characterized. For this purpose, reference chemicals were used in the first step and nanomaterials in the second step.

In order to ensure that the nebulization process itself has no influence on the viability of the treated cells and their morphology, A549 cells, which were cultured in the 96-well plates at ALI for 24 h prior to exposure, were treated with cell culture medium without any supplements or test materials sequentially up to 10 cycles of exposure. With the increasing number

of nebulizations, no effect on the cell viability was determined (**Figure 6**A). The same result can be observed when dimethyl sulfoxide (DMSO) containing cell culture medium is sequentially nebulized (Figure S7, Supporting Information). DMSO is a widely used organic solvent that is also used in cell biology for the preparation of poorly soluble substances, such as Bortezomib in this study, and can thus be present in low concentrations in the cell culture medium.
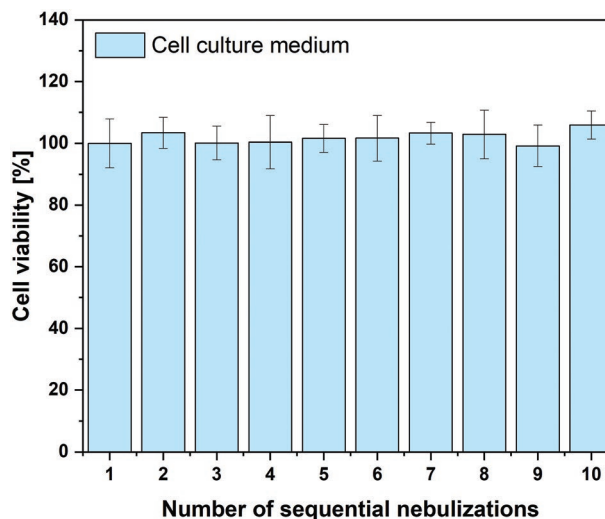

Figure 6. Effect of cell culture medium nebulization on human lung epithelial cells. A549 cells cultured as ALI model were exposed with FCS-free cell culture medium without any supplements. The cells were exposed up to ten times and its viability was calculated in relation to the untreated control cells. The cell viability was quantified based on metabolic activity analysis (alamarBlue assay). Mean values of three independent experiments (± standard deviation) are presented.

ADVANCED
SCIENCE NEWS
www.advancedsciencenews.com

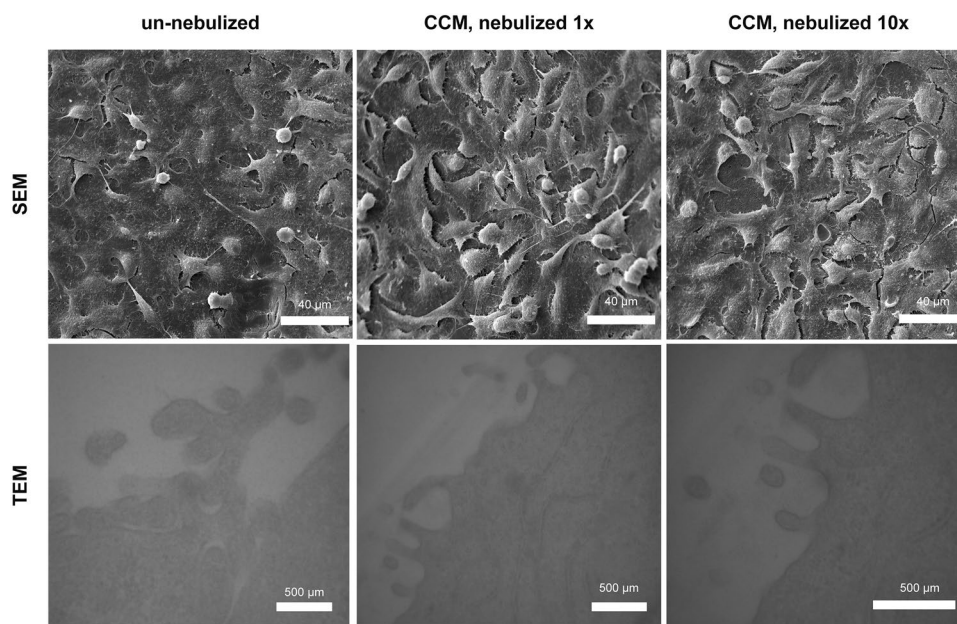NANO · MICRO
small
www.small-journal.com

Figure 7. Electron microscopic characterization of human lung epithelial cells after nebulized cell culture medium (CCM) exposure in the 96-well exposure system. Upper row: scanning electron microscopy (SEM) indicates the dense monolayer of the flat epithelial cells with microvilli on the apical side. Bottom row: transmission electron microscopy (TEM) of A549 cells. Microvilli are visible under each tested condition.

The cell morphology was also not affected by the multiple nebulizations of cell culture medium. Even after 10 nebulizations, the characteristics of the lung epithelial cells, such as microvilli, are clearly visible (**Figure 7**). SEM images identified the confluent layer with characteristic flat epithelial cells as a monolayer and TEM images clearly show apical microvilli (Figure 7).

2.4.1. Characterization with Reference Chemicals

Before the platform was used for cell-based in vitro studies with nanomaterials, the system was characterized with a number of reference chemicals. For this purpose, A549 cells, which were cultured in the 96-well plates at ALI for 24 h prior to exposure, were treated with 1 wt% TritonX and 200 μM Bortezomib sequentially up to 10 cycles of exposure. The deposited mass of both chemicals could be measured by the QCM and increases almost linearly with an increasing number of exposure cycles (**Figure 8**). In the case of TritonX, the cell viability decreased with an increasing dose (Figure 8), whereas Bortezomib does not induce loss of metabolic activity of the cells (Figure 8).

TritonX is a detergent, which irreversibly disrupts cell membranes and consequently induces cell death.[67] This chemical-induced effect can be clearly replicated in the 96-well exposure system, since A549 cells lose their viability with increasing dose of TritonX (Figure 8A1). Bortezomib is a cytostatic drug, whose effect is based on the inhibition of proteasomes, which degrade damaged proteins by proteolysis.[68] Since the used viability assay is based on the reduction of resazurin to resorufin by metabolic active cells, it does not correlate with the proteolytic activity of the cells. Based on this, no effect on

the mitochondrial cell metabolic activity is observed, even with increasing doses of Bortezomib (Figure 8B).

2.4.2. Effect of AgNP and CNC on ALI Culture in 96-Well Format

After characterizing the system with reference chemicals, A549 cells were cultured as ALI in the 96-well plate and as the next step, these cells were exposed to spherical Ag-NP (20 μg mL^{-1}) and the synthesized rod-shaped CNC (22 mg mL^{-1}). The deposited mass of both nanomaterials was measured by the QCM and increased nearly linearly with an increasing number of exposure cycles (**Figure 9**). None of the tested nanomaterials induce loss of metabolic activity of the cells at any of the delivered doses. Unlike a number of in vitro studies that report strong cytotoxicity of applied Ag-NP suspensions, Ag-NP applied as an aerosol to cells cultured at ALI is negligibly cytotoxic and only induces mild inflammatory effects.[69,70] It has been shown in many nanotoxicity studies that aerosol exposure induces different biological answers than submerged exposures,[58,62,71,72] which is in line with the results of this study. In addition to the study of cell viability, the morphology of the cells was investigated via TEM and SEM. Compared to the untreated control and the cells nebulized several times with pure CCM (Figure 7), the cells exposed to Ag-NP no longer showed a homogeneous cell layer after tenfold nebulization. Individual nanoparticles could be found inside the cells, which proves the uptake of Ag-NP into the cells (**Figure 10**). Cell morphology was also not affected by the multiple nebulizations of CNC (Figure 10). Even after 10 nebulizations, the characteristic microvilli are clearly visible on the surface of the lung epithelial cells (Figure 10). TEM

ADVANCED
SCIENCE NEWS
www.advancedsciencenews.com

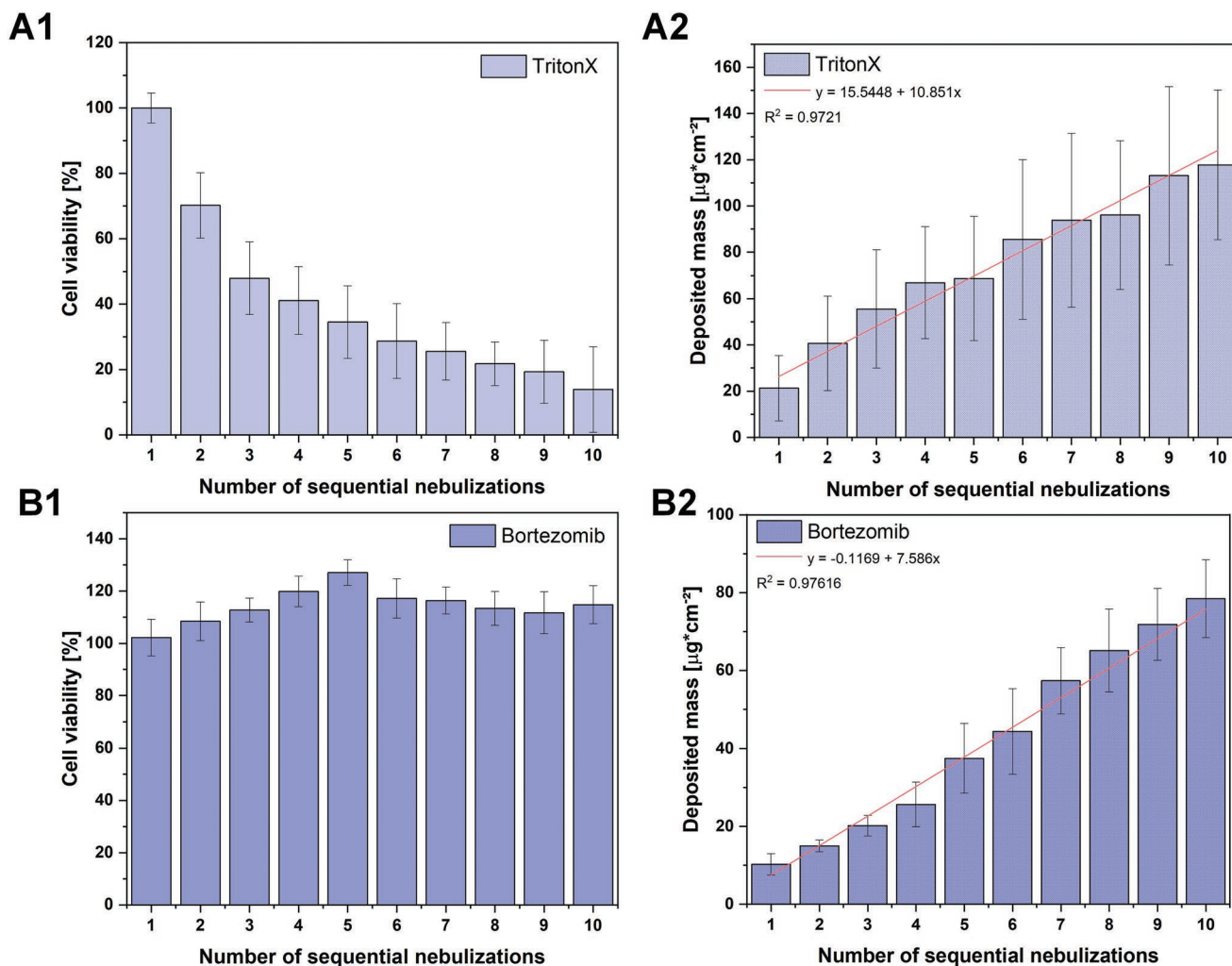NANO · MICRO
small
www.small-journal.com

Figure 8. Characterization of the 96-well exposure system with chemicals. A549 cells cultured as ALI model were exposed with A) 1 wt% TritonX or B) 200 μm Bortezomib. In parallel to the exposure the deposited mass was measured by QCM (A2, B2). The cell viability was quantified based on metabolic activity analysis (alamarBlue assay) (A1, B1). Mean values of three independent experiments (± standard deviation) are presented.

images identified vesicles in which CNC seems to be incorporated (Figure 10).

As Ag-NP are biologically well-characterized nanomaterials, little is known to date about the potential biological effects of CNC extracted from cellulose. CNC is a key player in the development of advanced materials due to their outstanding physical and chemical properties.[37–41] These kinds of particles, with typical dimensions of 4–20 nm in width and 100–500 nm in length[73] are found in a wide range of industrial applications, such as polymer composites or in cosmetic and medical products.[42] Nevertheless, to date, only a few studies have investigated the toxicity of CNC on lung cell function.[43,74,75]

Published toxicological studies with nanocellulose, in vitro[75,76–79] and in vivo[43,80–82] show a distinct lack of coherent data to substantially assess and target the toxicological potential of CNC. The published studies indicate that the physicochemical properties of CNC, particularly the agglomeration state and aspect ratio, influence their biological effects.[83–85] However, a way to predict toxicity as a function of CNC physico-chemical properties has not yet been reported. In the present study, an increased dose of CNC delivered as an aerosol to A549 cells, induces no decrease in metabolic activity using 22 mg mL^{-1} CNC (Figure 9B1). This is in contrast to recently published animal studies conducted in rats, where CNC inhalation caused lung toxicity by inflammation and oxidative stress.[36] However, rats were exposed for 6 h a day for a total of 14 days, which cannot be compared with the dose delivered in the presented in vitro 96-well exposure system. Another study, in which a lower dose was delivered to mice twice a week over 3 weeks, also reported lung damage induced by inflammation and oxidative stress after CNC exposure.[86] Occasional in vitro studies have reported lower cytotoxities of CNCs than multi-walled carbon-nanotubes on a 3D, co-culture, lung model,[77] and referred to the aspect of length and concentration of cellulose nanofibers in the context of interaction with lung cells.[78] Besides the influence of nanocellulose on inflammatory processes and oxidative stress, they have also been discussed as a possible trigger of genotoxic effects.[76,87–94]
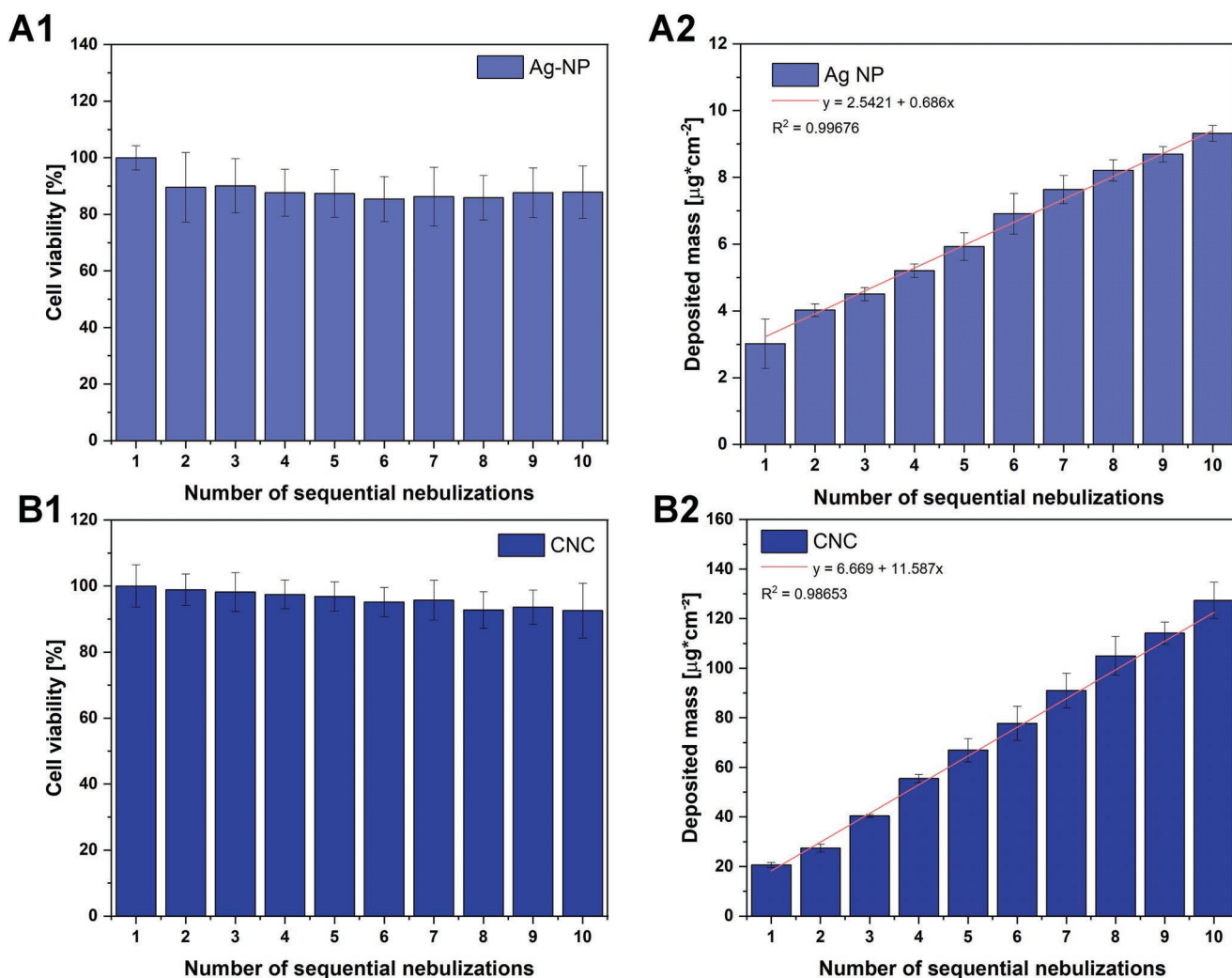
Figure 9. Characterization of the 96-well exposure system with nanomaterials. A549 cells cultured at ALI were exposed with A) 20 µg mL^{-1} Ag-NP or B) 22 mg mL^{-1} CNC. In parallel to the exposure the deposited mass was measured by QCM (A2, B2). Cell viability was quantified based on metabolic activity analysis (A1, B1). Mean values of three independent experiments ± standard deviation are presented.

3. Conclusion

The goal of this study was to develop and characterize a 96-well aerosol exposure system for the safety assessment of nanomaterials. For this purpose, an exposure system for sequential nebulization in a 96-well format was designed, fabricated, and characterized using an ALI lung epithelial model. This 96-well exposure system was developed with the capability of sequential exposure of individual rows of wells with test substances as aerosols, thus offering the possibility of creating dose-response curves using the system. This allows the generation of a more reliable cell-based assay data for many types of applications, such as safety analysis (endpoint and toxicokinetic studies), disease modeling, drug efficacy testing, or chemical registration within REACH (Registration, Evaluation, Authorisation and Restriction of Chemical Substances).[95]

The presented results show that the developed exposure system can be used for dose-response studies of drugs, chemicals, and nanomaterials with simple, but also complex morphology on an ALI epithelial model in a 96-well format. The integration of a QCM in the base module allows a method for accurate dosimetry measurement of deposited mass on the cells.

The comparison of the application modes clearly indicated that a sequential application produces very good distribution profiles (both within a row of wells and between the wells). This is valid not only for the distribution of large molecular structures, such as fluorescein sodium, but also for morphologically complex nanoparticulate structures, such as CNC. Thus, the system is suitable for the application of drugs and chemicals but also for the homogeneous distribution of nanomaterials. A negative influence, such as agglomeration effects on the nebulization process on the morphology of the particles could be excluded. The design of the exposure system is obviously suitable for the cultivation and exposure of any ALI model and is not limited to lung in vitro models. Although the cloud system is mainly used for lung exposure studies, the method is also suitable for the application of ALI cultured skin cell models.[96]
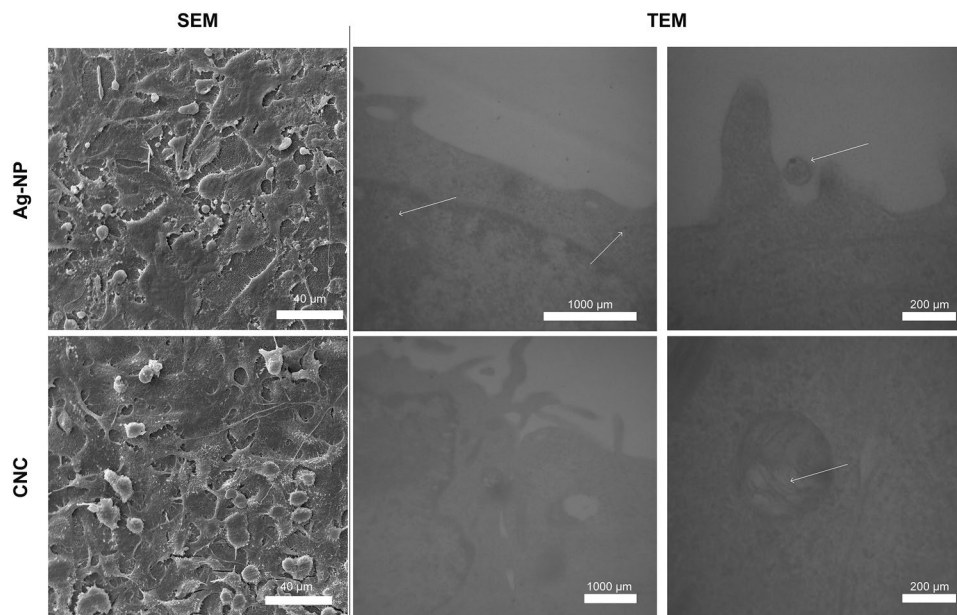
**ADVANCED
SCIENCE NEWS**

www.advancedsciencenews.com

**NANO · MICRO
small**

www.small-journal.com

Figure 10. Electron microscopic characterization of human lung epithelial cells after nebulized cell culture medium (CCM) exposure in the 96-well exposure system. Upper row: A549 cells (cultured as ALI model) after 10× exposure with 20 μg mL^{-1} Ag-NP (upper row) or 22 mg mL^{-1} CNC (bottom row). The cells were analyzed with scanning electron microscopy (SEM) and transmission electron microscopy (TEM).

After successful characterization with this first set of chemicals, drugs, and nanomaterials, future steps include combination of the system with other cell models, such as human induced pluripotent stem cells[97–99] or reporter cells,[100] for example.

In all fields of application this in vitro technique offers new perspectives on in vivo-like and animal-free approaches and contributes to the replacement of animal testing in safety assessment studies in compliance with the 3Rs principles of replacing and reducing animal experiments.

4. Experimental Section

Setup of the 96-Well Exposure System for Nebulization of Test Substances: The exposure system (Cloud Alpha SEQ 96, VITROCELL Systems, Waldkirch, Germany) was set up using a series of different components. The aerosol chamber (length × width × height = 16.0 × 12.5 × 15.1 cm) was equipped with a Aeroneb Pro vibrating mesh nebulizer (Aerogen Inc., Galway, Ireland) centrally located on top of the chamber. The nebulizer generates droplets with an aerodynamic diameter of 4–6 μm. An aerosol outlet on the nebulizer mounting was connected to a vacuum pump (Laboport N820G, KNF, Germany). The heatable base module contains a 96-well stainless steel plate, which was filled with cell culture medium and into which the 96-well insert plate (Merck, Darmstadt, Germany) was positioned. The dimensions of the insert plate were 12.1 × 7.3 cm with a surface area for cell growth of 0.143 cm^2 per well. It was covered with a 96-well silicone seal and a flat 96-well stainless steel plate on top. For sequential dosing, a row of 8-wells can be covered by a manually movable stainless steel sliding panel, enabling the coverage of one to twelve rows. Silicone seals on the lower side of the sliding panel seal the wells tightly to keep aerosol from entering. The base module holds another insert for a 6-well QCM. The total surface area of the base being exposed to the aerosol was 190 cm^2.
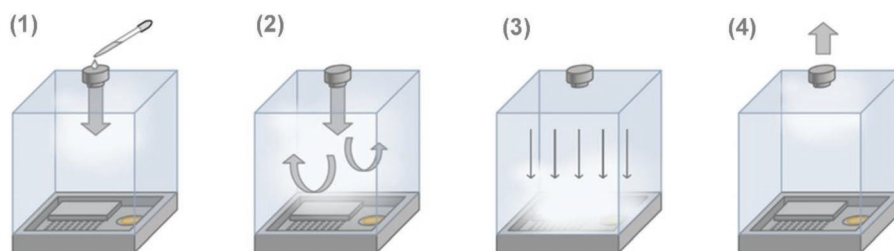
The principle of the sequential mode exposure feature is schematically depicted in **Figure 11**. The test substance was dissolved in an aqueous solution and pipetted onto the vibrating mesh nebulizer on top of the exposure chamber. The nebulizer emits a dense cloud of droplets. Due to the formation of vortices at the bottom of the chamber, the cloud was convectively mixed into a uniform mist, gradually filling the entire exposure chamber from bottom up. Subsequent sedimentation of this mist results in uniform aerosol deposition onto the cells located at the bottom of the exposure chamber. Implementation of a QCM in the base module allows a method for accurate dosimetry measurement of deposited mass on the cells.[47,64] Repeated runs of nebulization were performed (Figure 11). For sequential dosing, the slide panel initially covers all rows, except for row 1. Before each exposure the slide panel, covering the cell culture plate, was removed sequentially (Figure 11). Only the rows which were not covered were exposed to the aerosol. Thus, the deposited mass on the already exposed rows continually increases with each exposure resulting in different dosing of the test substance on the cell cultures. In order to remove aerosol residues after sedimentation of the aerosol, the chamber was evacuated with vacuum with a low flow rate.

Cell-Free Characterization with Fluorescein Sodium and CNC-AF488: Cell-free experiments were conducted with aerosolized fluorescein sodium salt (Merck, Darmstadt, Germany) dissolved in phosphate buffered saline (Merck, Darmstadt, Germany) and CNC-AF488.

For the non-sequential-mode a concentration of 30 μg mL^{-1} fluorescein sodium salt was used. For the sequential mode 15 μg mL^{-1} fluorescein sodium salt was used to stay under saturation. 500 μL of the solution was nebulized per exposure. After each exposure, the aerosol was maintained in the chamber for 7 min before being evacuated by a gentle vacuum flow for 60 s. The fluorescein sodium was trapped in 40 μL phosphate buffered saline aliquoted onto the membrane of each well of a 96-well insert plate (3381, Corning; Amsterdam, Netherlands) prior to nebulization, as trapping liquid. After the last exposure, 30 μL of the trapping liquid of each well was mixed and transferred to a black 96-well half area plate (3694, Corning, Amsterdam, Netherlands), respectively. In this experiment, the QCM was not used. Fluorescence intensity was measured via fluorescence spectrometry (excitation, 483 nm; emission, 530 nm; CLARIOstar Plus, BMG LABTECH, Ortenberg, Germany) using MARS Data Analysis Software (BMG LABTECH, Ortenberg, Germany) for analysis. 1) Mean mass values of fluorescein sodium deposited

ADVANCED
SCIENCE NEWS
www.advancedsciencenews.com

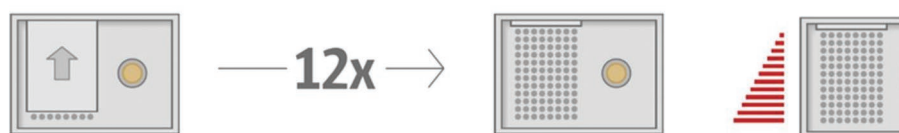NANO · MICRO
small
www.small-journal.com

Figure 11. Working principle of the sequential mode feature of the 96-well exposure system. The 96-well insert plate with cells cultured at the air–liquid interface is placed in the base module. For sequential dosing, the slide panel initially covers all rows, except for row 1. The test substance is dissolved in an aqueous solution and pipetted onto the vibrating mesh nebulizer on top of the exposure chamber. The nebulizer emits a dense cloud of droplets. Due to convective mixing by vortices the cloud transforms into a uniform mist of droplets, settling spatially uniform onto the bottom of the chamber. The cells not being covered by the slide panel are continuously exposed to the aerosol. After sedimentation residual aerosol is removed from the chamber using a vacuum with a low flow rate. Before each exposure, the sliding panel is removed sequentially row-by-row resulting in 12 different dose levels.

per cm^2, 2) deposition efficiency, and 3) insert-to-insert-variability were calculated for each setting as follows:

$$\text{Mass deposition}\left[\mu\text{gcm}^{-2}\right] = \frac{\sum\left(c_{\text{insert}} \times V_{\text{trapping}}\right)}{\gamma} \cdot \frac{1}{A_{\text{insert}}} \quad (1)$$

$$\text{Deposition efficiency}\left[\%\right] = \frac{c_{\text{insert}} \times V_{\text{trapping}}}{c_{\text{nebulized}} \times V_{\text{nebulized}}} \cdot \frac{A_{\text{chamber}}}{A_{\text{insert}}} \cdot 100\% \quad (2)$$

$$\text{Insert-to-insert-variability}\left[\%\right] = \sqrt{\frac{\sum\left(c_{\text{insert}} - c_{\text{av}}\right)^2}{\gamma}} \cdot \frac{1}{c_{\text{av}}} \cdot 100\% \quad (3)$$

with c_{insert}: Fluorescein sodium concentration deposited in each insert [μg mL^{-1}], c_{av}: Mean fluorescein sodium concentration [μg mL^{-1}], $c_{\text{nebulized}}$: Concentration of fluorescein sodium in nebulized liquid [μg mL^{-1}], V_{trapping}: Volume of trapping liquid in each insert [mL], $V_{\text{nebulized}}$: Volume of nebulized liquid per dose [mL], A_{insert}: Inner surface area of insert [cm^2], A_{chamber}: Surface area of the base of the chamber [cm^2], γ: Number of inserts per dose, n: Number of experiments.

CNC-AF488 stock solution (22 mg mL^{-1}) was diluted in phosphate buffered saline to a concentration of 10 mg mL^{-1} and aerosolized in sequential mode. 200 μL of the solution was nebulized per exposure. 80 μL supernatant was collected from each well and transferred to a black, 96-well plate, with a clear bottom (#655090, Greiner BioOne, Germany) for fluorescence measurement, using a Tecan Infinite F200 plate reader (Tecan, Maennedorf, Switzerland) at an excitation/emission wavelength of 485/535 nm.

Materials for Synthesis of CNC and CNC-AF488: Hardwood pulp (Guaíba, obtained from eucalyptus and blackwood acacia) was provided by GRÜNPERGA Papier GmbH (Grünhainichen, Germany) and used as cellulose raw material. Sulfuric acid (H$_2$SO$_4$, 96 wt%) for CNC extraction was purchased from Carl Roth (Karlsruhe, Germany). Deionized water (18.2 MΩ·cm, Milli-Q Direct 8 water purification system, Merck Chemicals, Schwalbach, Germany) was used throughout the experiment. 3-aminopropyltriethoxysilan (APTES) 99 wt%, H$_2$SO$_4$ 96 wt%, HCl 1 mol L^{-1}, NaOH 1 mol L^{-1}, Na$_2$CO$_3$ 99.5 wt%, NaHCO$_3$ 99.7 wt%, DMSO

99.9 wt%, and acetone were purchased from Sigma Aldrich (Darmstadt, Germany), AlexaFluor 488 NHS ester (AF488-NHS) from Click Chemistry Tools (Scottsdale, Arizona/USA).

Reagents for In Vitro Studies: TritonX-100 (T8787-50ML), Bortezomib (Calbiochem 179324-69-7), and Ag-NP dispersion (730785) were purchased from Sigma Aldrich (Darmstadt, Germany). All reagents were diluted in FCS-free cell culture medium before nebulization. In the cases of Ag-NP and CNC, 0.02 mg mL^{-1} stock solution or 22 mg mL^{-1} stock solution, respectively, were nebulized.

Extraction of Nanocrystalline Cellulose: Nanocrystalline cellulose (CNC) was extracted from hardwood pulp by sulfuric acid hydrolysis, following the protocol of Cranston and Gray with minor modifications.[101,102] Sulfuric acid (diluted to 62 wt% with deionized water) was pre-heated to 44 °C in a stirred tank reactor (Atlas, Syrris, Royston, UK) equipped with an anchor-type stirrer. Cellulose raw material (previously dried at 105 °C for 30 min) was then added at a ratio of 1/10 (cellulose/sulfuric acid, w/w).[102] The reaction mixture was stirred constantly at 200 rpm for 40 min. Afterward, the reaction was quenched by tenfold dilution with deionized water. Centrifugation was carried out for 15 min at a relative centrifugal force of 4594 rcf (Centrifuge 5910 R, Eppendorf, Hamburg, Germany). The clear supernatant was discarded and the precipitate was redispersed in deionized water and recentrifuged until peptization occurred. For further purification, the obtained suspension was dialyzed in regenerated cellulose tubes (ZelluTrans/ROTH T3, Carl Roth, Karlsruhe, Germany). Agglomerates were broken via ultrasonication using a Sonopuls HD 3200 homogenizer equipped with a VS 70 T sonotrode (Bandelin, Berlin, Germany) at a specific energy of 2 kJ g^{-1} cellulose (as recommended by Beck et al.[103]) and an amplitude setting of 30% in an ice bath followed by centrifugation (4594 rcf, 15 min). The resulting aqueous CNC suspension (having a solid content of 1.9 – 2.2 wt%) was stored at 4 °C until further use.

Synthesis of Alexa488 Labeled CNC: Labeling of CNC was performed in a two-step-synthesis—in the first step, a primary amino group was introduced, which formed a conjugate (here an amide), then with the AF488-NHS in the second step.

In brief, the synthesis of the amino-conjugated CNC (CNC-NH$_2$) was conducted as follows (see also ref. [66]): The pH of 300 mL aqueous

ADVANCED
SCIENCE NEWS
www.advancedsciencenews.com

NANO · MICRO
small
www.small-journal.com

CNC suspension with 1 wt% was adjusted to 1.5 by addition of HCl (1 mol L⁻¹), followed by addition of 0.012 moles (2.7 mL) APTES whilst being vigorously stirred (hydrolysis step of APTES). After stirring for 30 min, the pH was adjusted to 10.5 by adding NaOH (1 mol L⁻¹) to the mixture, which was then left under constant stirring for 3 h (condensation step = formation of CNC-NH₂). Subsequent centrifugation and washing with mixtures of water and acetone, acetone, and water, with intermittent sonication periods, isolated the product CNC-NH₂ (2.7 wt% determined by drying method).

The conjugation of the AF488-NHS with CNC-NH₂ was performed as follows: 37 g CNC-NH₂ (2.7 wt% in water) was diluted with 63 g 0.1 M NaHCO₃/Na₂CO₃ buffer solution to achieve 100 g CNC-NH₂ (1.0 wt% in buffer, pH 9). 100 mg AF488-NHS were dissolved in 10 mL DMSO to achieve a concentration of 10 mg mL⁻¹ and added to the prepared CNC-NH₂ suspension. After stirring, in the dark, for 1 h at 4 °C, the conjugate product CNC-AF488 was centrifuged and washed several times with buffer solution and diluted to a final concentration of 1 wt%.

AF4-MALS: The samples were fractionated and subsequently characterized on a multi-detector AF4 system (AF2000 MT, Postnova Analytics GmbH (PN), Landsberg am Lech, Germany). The AF4 system was coupled with a UV/Vis detector (PN3211) and MALS detector (PN3621, 21 angles). The AF4 setup and fractionation conditions are described in detail in Metzger et al.[102] An analytical fractionation channel with a tip-to-tip length of 277 mm, which was equipped with a regenerated cellulose (RC) membrane of 10 kDa molecular weight cut-off and a Mylar spacer with 350 µm thickness, was used. The sample preparation for CNC-AF488 was performed as summarized in Campora et al.[66] CNC samples in cell culture medium were injected as received.

Single Particle ICP-MS Measurements: spICP-MS measurements were carried out on an Agilent ICP-MS 7900 (Agilent Technologies, Waldbronn, Germany) as described in Kohl et al.[104] In brief, the samples were introduced using an ASX-500 Autosampler (Agilent Technologies, Waldbronn, Germany) and a peristaltic pump operating at 0.1 rpm, which corresponds to a flow rate of 0.346 mL min⁻¹. Data were acquired for 60 s recording the intensities of the isotope 107 Ag at a dwell time of 100 µs.

Conductometric Titration: The surface charge density (OSO_3^-) of the CNC was determined via conductometric titration (Konduktometer 703 with an electrode sensor SE 204, Knick, Berlin, Germany) according to Beck et al.[103]

Electron Microscopy: TEM analysis of the un-nebulized CNC was performed as described by Campora et al.,[66] using a Philips CM10 instrument (FEI Eindhoven, Netherlands), coupled with a CCD camera (µ-Eye, IDS Imaging, Obersulm, Germany), at an acceleration voltage of 80 kV. A small droplet of each un-nebulized sample was placed on a carbon-coated copper TEM grid and left to dry at room temperature. Negative staining was carried out with a saturated ethanolic uranyl acetate solution. For TEM analysis of nebulized samples, they were nebulized (see procedure below) on a pioloform-coated copper grid (G2440C, Plano, Wetzlar, Germany) and prepared as in Campora et al.[66]

For electron microscopy investigation of the cells, cultured as ALI, were chemically fixed, dehydrated, embedded in resin, and sectioned as described previously (Kohl et al. 2021).[104] TEM investigation was also carried out by a Philips TEM CM10 at 80 kV. For scanning electron microscopy (SEM), the fixed and dehydrated cells were dried by critical point drying using a CPD 010 (Baltec, Pfäffikon, Switzerland). After drying, the samples were mounted on aluminum stubs (Plano, Wetzlar, Germany) and coated with gold using a sputter coater SCU 030 (Baltec, Pfäffikon, Switzerland). The investigations with the SEM DSM 940 (Zeiss, Oberkochen, Germany) were performed with 10 kV and the images were captured using the software DISS 5 (point electronic).

Dynamic Light Scattering: The hydrodynamic apparent particle size was determined by dynamic light scattering (DLS) using a Zetasizer Nano ZSP (Malvern Instruments, Worcestershire, UK) equipped with a red laser (633 nm) under a backscatter detection angle of 173°. The harmonic intensity-weighted average particle diameter (Z-average) and the polydispersity index (PDI) were obtained by cumulants analysis for samples diluted to 0.025 wt% with deionized water.[105]

FTIR Measurement: For characterization of the samples, Fourier-transform infrared spectroscopy (FTIR) was used. The Infrared spectroscopic analysis was performed on dry samples using a Perkin Elmer FT-IR in attenuated total reflection and GoldenGate system as sample holder. For the evaluation, a combined database system from Perkin Elmer, Nicodom, and Wiley was used.

ζ-Potential Measurement: The ζ-potential of CNC was measured by electrophoretic light scattering with a Zetasizer Nano ZSP (Malvern Instruments, Worcestershire, UK) using the Smoluchowski approximation. Measurements were performed on a 0.25 wt% CNC suspension in 1 mmol L⁻¹ potassium chloride. To determine the surface charge of CNC, CNC-AF488, and Ag-NP in cell culture media, the protocol reported by Elje et al.[106] was used.

Dosimetry Using QCM: After each exposure, the deposited mass of test substance (µg cm⁻²) was determined by the Monitor software (Vitrocell, Waldkirch, Germany) after the QCM was allowed to stabilize for 3 min (until QCM surface was dried).

Cell Lines and Standard Cell Cultivation: All cell culture reagents were obtained from Invitrogen (Karlsruhe, Germany), unless stated otherwise. Human lung epithelial carcinoma cells A549 (ATCC CCL-185, American Type Culture Collection, USA) were cultured in Roswell Park Memorial Institute (RPMI) 1640 medium supplemented with L-glutamine (4 mM), penicillin (100 U mL⁻¹), streptomycin (100 µg mL⁻¹), and 10% (v/v) fetal calf serum (FCS), as previously described by Kohl et al.[107] Cells were passaged twice a week and cultivated at 95% humidity, and 5% CO₂ at 37 °C.

ALI Formation in 96-Well Plates: A549 cells were seeded at a density of 1.5×10^4 per well in 96-well insert plates with a 0.4 µm pore sized polycarbonate membrane (3381, Corning, Amsterdam, Netherlands). Apical volume was 100 µL and basolateral chamber was prefilled with 200 µL cell culture medium. After a cultivation time of 24 h, apical medium was removed and cells were cultivated for further 24 h at ALI until the exposure was performed.

Exposure of ALI Model in the 96-Well Exposure System: Cells were exposed in sequential mode (11 exposures of single rows) of the 96-well exposure system to FCS-free cell culture medium without test substance (control), 1 wt% TritonX-100 in FCS-free cell culture medium, 200 µM Bortezomib in FCS-free cell culture medium, 7.7 µg mL⁻¹ DMSO in FCS-free cell culture medium (solvent of Bortezomid stock solution), 20 µg mL⁻¹ Ag-NP dispersion or 22 mg mL⁻¹ CNC dispersion. 200 µL of the test substance was nebulized with an Aeroneb Pro vibrating membrane nebulizer, which generates a dense cloud of droplets with a median aerodynamic diameter of 4.0–6.0 µm.[60] After a settling time of 5 min, remaining droplets were sucked out by a gentle vacuum flow for 60 s. Non-exposed cells (first row) served as negative control.

Viability Assay (alamarBlue) in 96-Well Insert Plates: After the exposure and 24 h incubation time, cells were incubated apically with 100 µL of working solution of alamarBlue (Invitrogen, USA) in cell culture medium without FCS for 1 h at 37 °C. 80 µL supernatant of each well was transferred to a black, 96-well, with a clear bottom (#655090, Greiner BioOne, Germany) for fluorescence measurement using a Tecan Infinite F200 plate reader (Tecan, Maennedorf, Switzerland) at an excitation/emission wavelength of 560/610 nm. Data evaluation was performed on Tecan i-control software (Version 1.9.17.0, Tecan, Maennedorf, Switzerland). Data calculation was performed using Excel (Microsoft Office 2016).

Statistical Analysis: Results of the physico-chemical characterization and the toxicology studies were presented as mean ± standard deviation of three independent experiments ($n = 3$), unless otherwise stated. Biological effects were compared to non-treated cells, and tested for statistical significance with GraphPad software. Diagrams were created with OriginPro, Version 2019 (OriginLab Corporation, Northampton, MA, USA).

Supporting Information

Supporting Information is available from the Wiley Online Library or from the author.

[1] M. Hittinger, N. Schneider-Daum, C. M. Lehr, *Eur. J. Pharm. Biopharm.* **2017**, *118*, 73.

[2] D. Primavessy, J. Metz, S. Schnur, M. Schneider, C. M. Lehr, M. Hittinger, *Eur. J. Pharm. Biopharm.* **2021**, *168*, 62.

[3] W. M. S. Russell, R. L. Burch, in *The Principles of Humane Experimental Technique*, Methuen & Co. Limited, London **1959**, p. 252.

[4] L. Díaz, E. Zambrano, M. E. Flores, M. Contreras, J. C. Crispín, G. Alemán, C. Bravo, A. Armenta, V. J. Valdés, A. Tovar, G. Gamba, J. Barrios-Payán, N. A. Bobadilla, *Rev. Invest. Clin.* **2020**, *73*, 199.

[5] K. C. Aske, C. A. Waugh, *EMBO Rep.* **2017**, *18*, 1490.

[6] S. Gordon, M. Daneshian, J. Bouwstra, F. Caloni, S. Constant, D. E. Davies, G. Dandekar, C. A. Guzma, E. Fabian, E. Haltner, T. Hartung, N. Hasiwa, P. Hayden, H. Kandarova, S. Khar, H. F. Kr, M. S. Marcel Leist, G. Lian, U. Marx, M. Metzger, K. Ott, P. Prieto, M. S. Roberts, E. L. Roggen, T. Tralau, C. van den Braak, H. Walles, C. M. Lehr, *Altern. Anim. Exp.* **2015**, *32*, 327.

[7] A. Moreira, M. Müller, P. F. Costa, Y. Kohl, *Adv. Biol.* **2022**, *6*, 2101139.

[8] C. V. Montefusco-Pereira, J. C. Horstmann, T. Ebensen, C. Beisswenger, R. Bals, C. A. Guzmán, N. Schneider-Daum, C. S. de Carvalho-Wodarz, C. M. Lehr, *J. Visualized Exp.* **2020**, *160*, e61069.

[9] P. S. Hiemstra, P. B. McCray, R. Bals, *Eur. Respir. J.* **2015**, *45*, 1150.

[10] L. Gribaldo, K. Hurley, P. Hiemstra, C. Greene, *Eur. Respir. J.* **2021**, *57*.

[11] S. G. Klein, T. Serchi, L. Hoffmann, B. Blömeke, A. C. Gutleb, *Part. Fibre Toxicol.* **2013**, *10*, 1901241.

[12] H. M. Braakhuis, S. K. Kloet, S. Kezic, F. Kuper, M. V. D. Z. Park, S. Bellmann, M. van der Zande, S. L.e Gac, P. Krystek, R. J. B. Peters, I. M. C. M. Rietjens, H. Bouwmeester, *Arch. Toxicol.* **2015**, *89*, 1469.

[13] H. Barosova, B. B. Karakocak, D. Septiadi, A. Petri-Fink, V. Stone, B. Rothen-Rutishauser, *Int. J. Mol. Sci.* **2020**, *21*, 5335.

[14] J. Metz, K. Knoth, H. Groß, C. M. Lehr, C. Stäbler, U. Bock, M. Hittinger, *Pharmaceutics* **2018**, *10*, 56.

[15] J. Susewind, C. De Souza Carvalho-Wodarz, U. Repnik, E. M. Collnot, N. Schneider-Daum, G. W. Griffiths, C. M. Lehr, *Nanotoxicology* **2016**, *10*, 53.

[16] J. D. Stucki, N. Hobi, A. Galimov, A. O. Stucki, N. Schneider-Daum, C.-M. Lehr, H. Huwer, M. Frick, M. Funke-Chambour, T. Geiser, O. T. Guenat, *Sci. Rep.* **2018**, *8*, 14359.

[17] N. T. Awatade, S. L. Wong, C. K. Hewson, L. K. Fawcett, A. Kicic, A. Jaffe, S. A. Waters, *Front. Pharmacol.* **2018**, *9*, 1429.

[18] L. J. Marshall, W. Oguejiofor, R. S. Willetts, H. R. Griffiths, A. Devitt, *J. Pharm. Pharmacol.* **2015**, *67*, 464.

[19] S. Steiner, S. Majeed, G. Kratzer, G. Vuillaume, J. Hoeng, S. Frentzel, *Toxicol. In Vitro* **2017**, *42*, 263.

[20] J. Zhang, U. Doshi, R. L. Wolz, P. Kosachevsky, M. J. Oldham, I. G. Gillman, K. M. Lee, *Toxicol. In Vitro* **2022**, *82*, 105352.

[21] D. Steinritz, N. Möhle, C. Pohl, M. Papritz, B. Stenger, A. Schmidt, C. J. Kirkpatrick, H. Thiermann, R. Vogel, S. Hoffmann, M. Aufderheide, *Chem.-Biol. Interact.* **2013**, *206*, 479.

[22] L. D. Chandrala, N. Afshar-Mohajer, K. Nishida, Y. Ronzhes, V. K. Sidhaye, K. Koehler, J. Katz, *Sci. Rep.* **2019**, *9*, 7263.

[23] M. Aufderheide, B. Halter, N. Möhle, D. Hochrainer, *BioMed Res. Int.* **2013**, *2013*, 734137.

[24] D. Ritter, J. Knebel, *Adv. Toxicol.* **2014**, *2014*, 185201.

[25] F. Cappellini, S. Di Bucchianico, V. Karri, S. Latvala, M. Malmlöf, M. Kippler, K. Elihn, J. Hedberg, I. O. Wallinder, P. Gerde, H. L. Karlsson, *Nanomaterials* **2020**, *10*, 618.

[26] K. Meldrum, J. A. Moura, S. H. Doak, M. J. D. Clift, *Nanomaterials* **2022**, *12*, 3431.

[27] P. P. H. Le Brun, A. H. De Boer, H. W. Frijlink, H. G. M. Heijerman, *Pharm. World Sci.* **2000**, *22*, 75.

[28] A. P. Roth, C. F. Lange, W. H. Finlay, *J. Aerosol. Med.* **2004**, *16*, 325.

[29] S. P. Hertel, G. Winter, W. Friess, *Adv. Drug Delivery Rev.* **2015**, *93*, 79.

[30] A. R. Martin, W. H. Finlay, *Expert Opin. Drug Delivery* **2015**, *12*, 889.

[31] T. B. Tilly, M. T. Nelson, K. B. Chakravarthy, E. A. Shira, M. C. Debrose, C. M. Grabinski, R. L. Salisbury, D. R. Mattie, S. M. Hussain, *Chem. Res. Toxicol.* **2020**, *33*, 1179.

[32] T. H. Tulchinsky, E. A. Varavikova, in *The New Public Health (Third Edition)*, Academic Press, **2014**, pp. 237–309.

[33] K. S. Vanka, S. Shukla, H. M. Gomez, C. James, T. Palanisami, K. Williams, D. C. Chambers, W. J. Britton, D. Ilic, P. M. Hansbro, J. C. Horvat, *Eur. Respir. Rev.* **2022**, *31*, 210250.

[34] S. Bakand, A. Hayes, F. Dechsakulthorn, *Inhalation Toxicol.* **2012**, *24*, 125.

[35] J. Yi, B. T. Chen, D. Schwegler-Berry, D. Frazer, V. Castranova, C. McBride, T. L. Knuckles, P. A. Stapleton, V. C. Minarchick, T. R. Nurkiewicz, *J. Visualized Exp.* **2013**, *75*, e50263.

[36] P. Joseph, C. M. Umbright, J. R. Roberts, J. L. Cumpston, M. S. Orandle, W. G. McKinney, T. M. Sager, *Inhalation Toxicol.* **2021**, *33*, 66.

[37] F. A. G. S. Silva, F. Dourado, M. Gama, F. Poças, *Nanomaterials* **2020**, *10*, 2041

[38] D. Trache, A. F. Tarchoun, M. Derradji, T. S. Hamidon, N. Masruchin, N. Brosse, M. H. Hussin, *Front. Chem.* **2018**, *8*, 392.

[39] P. Mali, A. P. Sherje, *Carbohydr. Polym.* **2022**, *275*, 118668.

[40] C. Metzger, H. Briesen, *Macromol. Mater. Eng.* **2021**, *306*, 2100161.

[41] C. Metzger, S. Sanahuja, L. Behrends, S. Sängerlaub, M. Lindner, H. Briesen, *Coatings* **2018**, *8*, 142.

[42] L. Bacakova, J. Pajorova, M. Bacakova, A. Skogberg, P. Kallio, K. Kolarova, V. Svorcik, *Nanomaterials* **2019**, *9*, 164.

[43] N. Yanamala, M. T. Farcas, M. K. Hatfield, E. R. Kisin, V. E. Kagan, C. L. Geraci, A. A. Shvedova, *ACS Sustainable Chem. Eng.* **2014**, *2*, 1691.

[44] E. R. Kisin, N. Yanamala, D. Rodin, A. Menas, M. Farcas, M. Russo, S. Guppi, T. O. Khaliullin, I. Iavicoli, M. Harper, A. Star, V. E. Kagan, A. A. Shvedova, *Chemosphere* **2020**, *250*, 126170.

[45] F. Pinto, A. F. Lourenço, J. F. S. Pedrosa, L. Gonçalves, C. Ventura, N. Vital, A. Bettencourt, S. N. Fernandes, R. R. da Rosa, M. H. Godinho, H. Louro, P. J. T. Ferreira, M. J. Silva, *Nanomaterials* **2022**, *12*, 1432.

[46] A. G. Lenz, E. Karg, B. Lentner, V. Dittrich, C. Brandenberger, B. Rothen-Rutishauser, H. Schulz, G. A. Ferron, O. Schmid, *Part. Fibre Toxicol.* **2009**, *6*, 32.

[47] A. G. Lenz, T. Stoeger, D. Cei, M. Schmidmeir, N. Semren, G. Burgstaller, B. Lentner, O. Eickelberg, S. Meiners, O. Schmid, *Am. J. Respir. Cell Mol. Biol.* **2014**, *51*, 526.

[48] C. Méausoone, R. El Khawaja, G. Tremolet, S. Siffert, R. Cousin, F. Cazier, S. Billet, D. Courcot, Y. Landkocz, *Toxicol. In Vitro* **2019**, *58*, 110.

[49] M. Pardo, S. Offer, E. Hartner, S. Di Bucchianico, C. Bisig, S. Bauer, J. Pantzke, E. J. Zimmermann, X. Cao, S. Binder, E. Kuhn, A. Huber, S. Jeong, U. Käfer, E. Schneider, A. Mesceriakovas, J. Bendl, R. Brejcha, A. Buchholz, D. Gat, T. Hohaus, N. Rastak, E. Karg, G. Jakobi, M. Kalberer, T. Kanashova, Y. Hu, C. Ogris, A. Marsico, F. Theis, et al., *Environ. Int.* **2022**, *166*, 107366.

[50] S. Binder, X. Cao, S. Bauer, N. Rastak, E. Kuhn, G. C. Dragan, C. Monsé, G. Ferron, D. Breuer, S. Oeder, E. Karg, M. Sklorz, S. Di Bucchianico, R. Zimmermann, *Environ. Mol. Mutagen.* **2021**, *62*, 490.

[51] B. M. Keyser, R. Leverette, M. Hollings, A. Seymour, R. A. Weidman, C. J. Bequette, K. Jordan, *Appl. In Vitro Toxicol.* **2022**, *8*, 39.

[52] J. Candeias, E. J. Zimmermann, C. Bisig, N. Gawlitta, S. Oeder, T. Gröger, R. Zimmermann, C. B. Schmidt-Weber, J. Buters, *Environ. Res.* **2022**, *211*, 112968.

[53] S. Offer, E. Hartner, S. Di Bucchianico, C. Bisig, S. Bauer, J. Pantzke, E. J. Zimmermann, X. Cao, S. Binder, E. Kuhn, A. Huber, S. Jeong, U. Käfer, P. Martens, A. Mesceriakovas, J. Bendl, R. Brejcha, A. Buchholz, D. Gat, T. Hohaus, N. Rastak, G. Jakobi, M. Kalberer, T. Kanashova, Y. Hu, C. Ogris, A. Marsico, F. Theis, M. Pardo, T. Gröger, et al., *Environ. Health Perspect.* **2022**, *130*, 27003.

[54] S. Oeder, T. Kanashova, O. Sippula, S. C. Sapcariu, T. Streibel, J. M. Arteaga-Salas, J. Passig, M. Dilger, H. R. Paur, C. Schlager, S. Mülhopt, S. Diabaté, C. Weiss, B. Stengel, R. Rabe, H. Harndorf, T. Torvela, J. K. Jokiniemi, M. R. Hirvonen, C. Schmidt-Weber, C. Traidl-Hoffmann, K. A. BéruBé, A. J. Wlodarczyk, Z. Prytherch, B. Michalke, T. Krebs, A. S. H. Prévôt, M. Kelbg, J. Tiggesbäumker, E. Karg, et al., *PLoS One* **2015**, *10*, e0126536.

[55] M. M. Leroux, R. Hocquel, K. Bourge, B. Kokot, H. Kokot, T. Koklič, J. Štrancar, Y. Ding, P. Kumar, O. Schmid, B. H. Rihn, L. Ferrari, O. Joubert, *Nanomaterials* **2022**, *12*, 1362.

[56] S. Murugadoss, S. Mülhopt, S. Diabaté, M. Ghosh, H. R. Paur, D. Stapf, C. Weiss, P. H. Hoet, *Nanomaterials* **2021**, *11*, 3226.

[57] M. Hufnagel, N. May, J. Wall, N. Wingert, M. Garcia-Käufer, A. Arif, C. Hübner, M. Berger, S. Mülhopt, W. Baumann, F. Weis, T. Krebs, W. Becker, R. Gminski, D. Stapf, A. Hartwig, *Nanomaterials* **2021**, *11*, 1685.

[58] E. I. Medina-Reyes, N. L. Delgado-Buenrostro, D. L. Leseman, A. Déciga-Alcaraz, R. He, E. R. Gremmer, P. H. B. Fokkens, J. O. Flores-Flores, F. R. Cassee, Y. I. Chirino, *Toxicol. In Vitro* **2020**, *65*, 104798.

[59] I. Kooter, M. Ilves, M. Gröllers-Mulderij, E. Duistermaat, P. C. Tromp, F. Kuper, P. Kinaret, K. Savolainen, D. Greco, P. Karisola, J. Ndika, H. Alenius, *ACS Nano* **2019**, *13*, 6932.

[60] I. Fizeşan, S. Cambier, E. Moschini, A. Chary, I. Nelissen, J. Ziebel, J. N. Audinot, T. Wirtz, M. Kruszewski, A. Pop, B. Kiss, T. Serchi, F. Loghin, A. C. Gutleb, *Part. Fibre Toxicol.* **2019**, *16*, 14.

[61] E. Durantie, D. Vanhecke, L. Rodriguez-Lorenzo, F. Delhaes, S. Balog, D. Septiadi, J. Bourquin, A. Petri-Fink, B. Rothen-Rutishauser, *Part. Fibre Toxicol.* **2017**, *14*, 49.

[62] T. Loret, E. Peyret, M. Dubreuil, O. Aguerre-Chariol, C. Bressot, O. le Bihan, T. Amodeo, B. Trouiller, A. Braun, C. Egles, G. Lacroix, *Part. Fibre Toxicol.* **2016**, *13*, 58.

[63] S. Steiner, S. Ferreira, A. Baldi, A. K. Kuczaj, S. Frentzel, M. Peitsch, J. Hoeng, R. Pmi, *P. M. P. S. A* **2019**, *51*, 369.

[64] Y. Ding, P. Weindl, A. G. Lenz, P. Mayer, T. Krebs, O. Schmid, *Part. Fibre Toxicol.* **2020**, *17*, 44.

[65] M. Röhm, S. Carle, F. Maigler, J. Flamm, V. Kramer, C. Mavoungou, O. Schmid, K. Schindowski, *Int. J. Pharm.* **2017**, *532*, 537.

[66] L. D. Campora, C. Metzger, S. Dähnhardt-Pfeiffer, R. Drexel, F. Meier, S. Fürtauer, *Polymers* **2022**, *14*, 1820.

[67] S. L. Regen, *JACS Au* **2020**, *1*, 3.

[68] K. Scott, P. J. Hayden, A. Will, K. Wheatley, I. Coyne, *Cochrane Database Syst. Rev.* **2016**, *20*, CD010816.

[69] A. L. Holder, L. C. Marr, *BioMed Res. Int.* **2013**, *2013*, 11.

[70] F. Herzog, M. J. D. Clift, F. Piccapietra, R. Behra, O. Schmid, A. Petri-Fink, B. Rothen-Rutishauser, *Part. Fibre Toxicol.* **2013**, *10*, 11.

[71] K. Lovén, J. Dobric, D. A. Bölükbas, M. Kåredal, S. Tas, J. Rissler, D. E. Wagner, C. Isaxon, *Nanotoxicology* **2021**, *15*, 494.

[72] A. Georgantzopoulou, T. Serchi, S. Cambier, C. C. Leclercq, J. Renaut, J. Shao, M. Kruszewski, E. Lentzen, P. Grysan, S. Eswara, J. N. Audinot, S. Contal, J. Ziebel, C. Guignard, L. Hoffmann, A. T. J. Murk, A. C. Gutleb, *Part. Fibre Toxicol.* **2016**, *13*, 1.

[73] T. V. Patil, D. K. Patel, S. D. Dutta, K. Ganguly, T. S. Santra, K. T. Lim, *Bioact. Mater.* **2022**, *9*, 566.

[74] T. Saito, S. Kimura, Y. Nishiyama, A. Isogai, *Biomacromolecules* **2007**, *8*, 2485.

[75] X. M. Dong, J. F. Revol, D. G. Gray, *Cellulose* **1998**, *5*, 19.

[76] J. Catalán, M. Ilves, H. Järventaus, K. S. Hannukainen, E. Kontturi, E. Vanhala, H. Alenius, K. M. Savolainen, H. Norppa, *Environ. Mol. Mutagen.* **2015**, *56*, 171.

[77] M. J. D. Clift, E. J. Foster, D. Vanhecke, D. Studer, P. Wick, P. Gehr, B. Rothen-Rutishauser, C. Weder, *Biomacromolecules* **2011**, *12*, 3666.

[78] C. Endes, S. Mueller, C. Kinnear, D. Vanhecke, E. J. Foster, A. Petri-Fink, C. Weder, M. J. D. Clift, B. Rothen-Rutishauser, *Biomacromolecules* **2015**, *16*, 1267.

[79] A. Albanese, P. S. Tang, W. C. W. Chan, *Annu. Rev. Biomed. Eng.* **2012**, *14*, 1.

[80] M. T. Farcas, E. R. Kisin, A. L. Menas, D. W. Gutkin, A. Star, R. S. Reiner, N. Yanamala, K. Savolainen, A. A. Shvedova, *J. Toxicol. Environ. Health, Part A* **2016**, *79*, 984.

[81] S. Il Jeong, S. E. Lee, H. Yang, Y. H. Jin, C. S. Park, Y. S. Park, *Mol. Cell. Toxicol.* **2010**, *6*, 370.

[82] R. Silva-Carvalho, J. P. Silva, P. Ferreirinha, A. F. Leitão, F. K. Andrade, R. M. Gil da Costa, C. Cristelo, M. F. Rosa, M. Vilanova, F. M. Gama, *Toxicol. Res.* **2019**, *35*, 45.

[83] K. A. Mahmoud, J. A. Mena, K. B. Male, S. Hrapovic, A. Kamen, J. H. T. Luong, *ACS Appl. Mater. Interfaces* **2010**, *2*, 2924.

[84] M. J. D. Clift, B. Rothen-Rutishauser, D. M. Brown, R. Duffin, K. Donaldson, L. Proudfoot, K. Guy, V. Stone, *Toxicol. Appl. Pharmacol.* **2008**, *232*, 418.

[85] Z. Hanif, F. R. Ahmed, S. W. Shin, Y. K. Kim, S. H. Um, *Colloids Surf., B* **2014**, *119*, 162.

[86] A. A. Shvedova, E. R. Kisin, N. Yanamala, M. T. Farcas, A. L. Menas, A. Williams, P. M. Fournier, J. S. Reynolds,

2207207 (14 of 15)

**ADVANCED
SCIENCE NEWS**

www.advancedsciencenews.com

NANO · MICRO
small

www.small-journal.com

D. W. Gutkin, A. Star, R. S. Reiner, S. Halappanavar, V. E. Kagan, *Part. Fibre Toxicol.* **2016**, *13*.

[87] S. Moreira, N. B. Silva, J. Almeida-Lima, H. A. O. Rocha, S. R. B. Medeiros, C. Alves, F. M. Gama, *Toxicol. Lett.* **2009**, *189*, 235.

[88] C. A. Poland, R. Duffin, I. Kinloch, A. Maynard, W. A. H. Wallace, A. Seaton, V. Stone, S. Brown, W. MacNee, K. Donaldson, *Nat. Nanotechnol.* **2008**, *3*, 423.

[89] A. B. Stefaniak, M. S. Seehra, N. R. Fix, S. S. Leonard, *Inhalation Toxicol.* **2014**, *26*, 733.

[90] M. Čolić, D. Mihajlović, A. Mathew, N. Naseri, V. Kokol, *Cellulose* **2015**, *22*, 763.

[91] T. Kovacs, V. Naish, B. O'Connor, C. Blaise, F. Gagné, L. Hall, V. Trudeau, P. Martel, *Nanotoxicology* **2010**, *4*, 255.

[92] R. de Lima, L. O. Feitosa, C. R. Maruyama, M. A. Barga, P. C. Yamawaki, I. J. Vieira, E. M. Teixeira, A. C. Corrêa, L. H. Caparelli Mattoso, L. F. Fraceto, *Int. J. Nanomed.* **2012**, *7*, 3555.

[93] K.-S. Hannukainen, S. Suhonen, K. Savolainen, H. Norppa, *Toxicol. Lett.* **2012**, *211*, S71.

[94] C. Ventura, C. Marques, J. Cadete, M. Vilar, J. F. S. Pedrosa, F. Pinto, S. N. Fernandes, R. R. da Rosa, M. H. Godinho, P. J. T. Ferreira, H. Louro, M. J. Silva, *J. Xenobiot.* **2022**, *12*, 91.

[95] E. Commission, *Regul. No 1907/2006 Eur. Parliam. Counc. Off. J. Eur. Union* **2006**, 219.

[96] E. Seurat, A. Verdin, F. Cazier, D. Courcot, R. Fitoussi, K. Vié, V. Desauziers, I. Momas, N. Seta, S. Achard, *Environ. Res.* **2021**, *196*, 110350.

[97] B. R. Dye, A. J. Miller, J. R. Spence, *Curr. Pathobiol. Rep.* **2016**, *4*, 47.

[98] S. Gotoh, I. Ito, T. Nagasaki, Y. Yamamoto, S. Konishi, Y. Korogi, H. Matsumoto, S. Muro, T. Hirai, M. Funato, S. I. Mae, T. Toyoda, A. Sato-Otsubo, S. Ogawa, K. Osafune, M. Mishima, *Stem Cell Rep.* **2014**, *3*, 394.

[99] M. Ghaedi, E. A. Calle, J. J. Mendez, A. L. Gard, J. Balestrini, A. Booth, P. F. Bove, L. Gui, E. S. White, L. E. Niklason, *J. Clin. Invest.* **2013**, *123*, 4950.

[100] L. C. Stoehr, C. Endes, I. Radauer-Preiml, M. S. P. Boyles, E. Casals, S. Balog, M. Pesch, A. Petri-Fink, B. Rothen-Rutishauser, M. Himly, M. J. D. Clift, A. Duschl, *Part. Fibre Toxicol.* **2015**, *12*, 29.

[101] E. D. Cranston, D. G. Gray, *Biomacromolecules* **2006**, *7*, 2522.

[102] C. Metzger, R. Drexel, F. Meier, H. Briesen, *Cellulose* **2021**, *28*, 10221.

[103] S. Beck, J. Bouchard, R. Berry, *Biomacromolecules* **2012**, *13*, 1486.

[104] Y. Kohl, M. Hesler, R. Drexel, L. Kovar, S. Dähnhardt-Pfeiffer, D. Selzer, S. Wagner, T. Lehr, H. von Briesen, F. Meier, *Nanomaterials* **2021**, *11*, 1358.

[105] M. S. Reid, M. Villalobos, E. D. Cranston, *Langmuir* **2017**, *33*, 1583.

[106] E. Elje, E. Mariussen, O. H. Moriones, N. G. Bastús, V. Puntes, Y. Kohl, M. Dusinska, E. Rundén-Pran, *Nanomaterials* **2020**, *10*, 545.

[107] Y. Kohl, M. Biehl, S. Spring, M. Hesler, V. Ogourtsov, M. Todorovic, J. Owen, E. Elje, K. Kopecka, O. H. Moriones, N. G. Bastús, P. Simon, T. Dubaj, E. Rundén-Pran, V. Puntes, N. William, H. von Briesen, S. Wagner, N. Kapur, E. Mariussen, A. Nelson, A. Gabelova, M. Dusinska, T. Velten, T. Knoll, *Small* **2021**, *17*, e2006012.